

Photoemission in the system of linear chains : application to $\text{PrBa}_2\text{Cu}_3\text{O}_7$ and $\text{La}_{2-x-y}\text{Nd}_y\text{Sr}_x\text{CuO}_4$

J.D. Lee, T. Mizokawa, and A. Fujimori

*Department of Complexity Science and Engineering and Department of physics, University of Tokyo, Bunkyo-ku,
Tokyo 113-0033, Japan
(November 16, 2018)*

Photoemission in the system of linear charged chains has been studied with the dipole matrix incorporated, from which its dependencies on the photoelectron momentum (\mathbf{k}), photon polarization ($\hat{\mathbf{E}}$), and photon energy (ω) can be explored. The used model is the three-dimensional array of non-interacting chains, which is so simple as to allow an analytic approach. Motivations of the study are for the doped CuO_3 chain in $\text{PrBa}_2\text{Cu}_3\text{O}_7$ and the doped static stripe phase in $\text{La}_{2-x-y}\text{Nd}_y\text{Sr}_x\text{CuO}_4$. The one-dimensional dispersion exhibiting spin-charge separation and its dependence on the momentum perpendicular to the chain and its $\hat{\mathbf{E}}$ -dependency as well are discussed in $\text{PrBa}_2\text{Cu}_3\text{O}_7$. For $\text{La}_{2-x-y}\text{Nd}_y\text{Sr}_x\text{CuO}_4$, the anomalous spectral distribution formed by two sets of stripes perpendicular to each other is investigated. The geometric effects led to by the dipole transition matrix including the interference of photocurrents from different chains are found to change the simple one-dimensional feature drastically. We find these changes are consistent with experiment for the chain system $\text{PrBa}_2\text{Cu}_3\text{O}_7$, but less satisfactory for the stripe phase in $\text{La}_{2-x-y}\text{Nd}_y\text{Sr}_x\text{CuO}_4$. This means that in the stripe phase much two-dimensional characters still exist unlike the chain system.

I. INTRODUCTION

Angle-resolved photoemission spectroscopy (ARPES) has become the most significant experimental tool for a search of the electronic structure, especially in the high temperature superconducting cuprates [1]. In many theoretical and experimental interpretations, the ARPES data is often compared to the one-electron spectral function $A(\mathbf{k}, \omega)$ or vice versa. For a more satisfactory description of the photoemission, i.e., if one is interested in various parameter dependencies or the line shapes of quasi-particle peaks, one must go beyond the spectral function [2]. For it, we may need to consider the photoexcitation process governed by the dipole transition matrix [3,4] and the extrinsic losses of the photoelectron on its way out to and through the surface [5,6]. In this paper, we give the study of transition matrix effects in the photoemission, while the extrinsic losses from the dynamical scattering are not our concern because their contributions are in many cases smaller by orders of magnitude.

The target systems are composed of charged linear chains, i.e., one-dimensional metals. One-dimensional metal has been known for the extreme realization of electron correlation effects in that there are an exotic spin-charge separation and only collective modes, not the single-particle excitation [7]. It has opened another paradigm different from Fermi liquid and is called Tomonaga-Luttinger liquid. In an actual situation, a one-dimensional metallic state is very unstable toward an insulating state or very marginal between metallic and insulating states through charge and spin ordering. Anyhow these one-dimensional chain systems have attracted considerable attentions especially since the dis-

covery of high T_C superconductors. Among the high T_C cuprates, $\text{YBa}_2\text{Cu}_3\text{O}_7$ (YBCO) and its family compounds have CuO_3 chain structure as well as CuO_2 plane. $\text{PrBa}_2\text{Cu}_3\text{O}_7$ (PBCO), among the YBCO family cuprates, does not support superconductivity unlike other cuprates, which is suggested due to the hole depletion in CuO_2 plane [8,9]. Additional holes are thought to be doped in the CuO_3 chain, not in the CuO_2 plane. In such a sense, PBCO can probably be an archetype of Tomonaga-Luttinger-type one-dimensional system, which has revived much interests in the study of metallic chain system within the study of high T_C cuprates (PBCO actually has a band gap opening possibly due to charge ordering in the chain [10]).

On the other hand, another feasible usefulness of the metallic chain system in high T_C superconductor physics is in the so called stripe phase observed in Nd-substituted $\text{La}_{2-x-y}\text{Nd}_y\text{Sr}_x\text{CuO}_4$ (Nd-LSCO) [11,12]. The stripe phase is due to the formation of an ordered array of charged stripes which are also antiphase domain walls between antiferromagnetic ordered spins in the CuO_2 planes, which gives the periodicity-doubling for spins compared to charges.

Recent ARPES experiments for PBCO [10] have shown actual evidence for one dimensionality immersed in, but distinguishable from contributions from the two-dimensional CuO_2 planes. In experiments, two kinds of dispersive band features are observed; one is from the undoped CuO_2 plane and the other is the doped CuO_3 chain. Especially in the one-dimensional-like features, the separation between charge and spin excitation is also suggested. It is a stimulating result of Tomonaga-Luttinger liquid that the low energy physics is dominated by uncoupled collective modes of charge and spin exci-

tations, also called holons and spinons. In experiments, it is also found that, in addition to the spin-charge separation, one-dimensional characters (particularly spinon parts) are strongly dependent on the photon polarization and at the same time on the momentum perpendicular to the chain. The results for PBCO should be also relevant to other one-dimensional insulator, SrCuO₂, which has a weakly coupled double Cu-O chain. It is very intriguing to find that the similar polarization and perpendicular momentum dependencies in ARPES are observed in SrCuO₂ as well [13]. These observations could be hardly explained by a single Tomonaga-Luttinger chain only, the additional effect probably needs incorporating, which motivated us to explore the dipole transition matrix related to the geometries of a chain system.

The static stripe phases in Nd-LSCO also lead to an interesting puzzle on the electronic structures through ARPES observations [14]. Prior to that, the neutron scattering experiments compellingly proposed that there should be the static stripe formation in Nd-LSCO and besides, the charged stripes be aligned with rotated by $\pi/2$ between two adjacent planes [12]. The low binding energy electronic structure actually looks more or less one-dimensional in the sense that the spectral weight distribution is roughly understood as a superposition of two perpendicular chains. However, the suppression of d -wave nodal signal along the Brillouin zone diagonal direction, particularly around the Γ point, could not be satisfactorily explained without additional physics. We suggest one necessary ingredient could be from the dipole transition matrix including the interferences from different stripes. Another noticeable point is that there have been no decisive evidences for Tomonaga-Luttinger liquid in the stripes phase unlike chains in PBCO. Therefore, in our study for Nd-LSCO, although we consider the matrix effects from one-dimensional system, we assume the simple Fermi liquid for a single stripe having well-defined Fermi point. Further, whether each stripe is a Fermi liquid or a Tomonaga-Luttinger liquid does not affect the conclusion of the present work because the calculated polarization and photon energy dependencies of ARPES spectra come from the matrix element effects reflecting the interference of photoelectrons from different stripes.

In this work, we account for the dipole matrix effects for the semi-infinite ($z > 0$) three-dimensional array of metallic chains, whose Green's function is considered. The slight photoelectron damping is taken into account in the simplest way. It is assumed that all the excitations including both charge and spin occur along the chain-direction, that is, the energy scale for the perpendicular excitation is very high. This means that we neglect the interchain (interstripe) interactions such as hybridization or Coulomb interaction, which may exist in the actual system and also the fluctuation of chain or stripe perpendicular to it, which could be important in a dynamical stripe phase. We think of two configurations. First, we simply model the three-dimensional array of chains for PBCO. On the other hand, for Nd-LSCO, we slightly ex-

tend the model and consider the three-dimensional chain array perpendicularly crossed in adjacent planes. For both configurations, the model is analytically tractable. The resulting spectra is determined by complicated interferences of chain contributions and thus the dipole matrix effects are geometric. The effects naturally give \mathbf{k} - and $\hat{\mathbf{E}}$ -dependent photoemission spectra, which is found consistent with the recent experiments.

The outline of this paper is as follows. First we discuss the basic theory and the suitable starting point to account for the dipole transition matrix in Sec. II. In Sec. III, we investigate the model for PBCO and discuss its results. We can see how the spectral function of Luttinger liquid changes by the transition matrix. Such changes are also found quite consistent with experiments. In Sec. IV, we extend and constitute the model for Nd-LSCO and obtain the spectral weight distribution through the similar type of calculation. The calculation is also more or less consistent with the low energy weight distribution in experiments (here we assume *a priori* metallic stripes) in a limited case, which is from the interference among chains. In the final Sec. V, we present the concluding remarks and give the outlook.

II. BASIC FORMALISM

To account for the dipole transition matrix in the photoemission spectral intensity, we follow Pendrey's formula [15]. Its benefit is to treat only one-particle Green's function without solving for any static stationary states. From Pendrey's the photoemission intensity $I(\mathbf{k}, E, \omega)$ is

$$I(\mathbf{k}, E, \omega) = -\frac{1}{\pi} \text{Im} M(\mathbf{k}, E, \omega),$$

$$M(\mathbf{k}, E, \omega) \equiv \langle \mathbf{k} | G^+(E + \omega) \Delta G^+(E) \Delta^\dagger G^-(E + \omega) | \mathbf{k} \rangle, \quad (1)$$

where G^\pm is the retarded or advanced one-particle Green's function and $|\mathbf{k}\rangle$ the photoelectron state. The photoelectron state could be represented as a plane wave in the lowest approximation, even if the real photoelectron wave function may be damped through the scattering with possible excitations in the solid, i.e., could be quite different from a plane wave except for in the very high energy region. In our study, assuming the solid occupies $z > 0$ space, we take into account the damping in the simplest way by taking the photoelectron wave as a plane wave in the in-plane direction and a damped wave in the z -direction. This would not be a very good representation due to the anisotropy inherent in the system even in the in-plane direction [16]. We would expect and show, nevertheless, this could catch the essential physics as it should have. Then in Eq.(1) we replace $|\mathbf{k}\rangle$ by $|\tilde{\mathbf{k}}\rangle$, which is given as

$$\langle \mathbf{r} | \tilde{\mathbf{k}} \rangle = \frac{1}{(2\pi)^{3/2}} e^{-i\mathbf{K}\cdot\mathbf{R}} [\theta(z) e^{-i\tilde{k}_z z} + \theta(-z) e^{-ik_z z}]. \quad (2)$$

\tilde{k}_z is a complex number, $\tilde{k}_z = \sqrt{k_z^2 + i\Gamma}$, and thus the photoelectron gets damped. It is worth noting that a damped photoelectron state is the formal solution of the one-electron Schrödinger equation

$$(\epsilon_{\mathbf{k}} - \mathcal{H}_0 - \Sigma)|\mathbf{k}\rangle = 0, \quad (3)$$

where Σ is the self-energy operator involving the photoelectron-solid interaction. Equation (2) can be understood from the first approximation for its self-energy, $\Sigma = -i\Gamma\theta(z)$. If we insert the plane wave states in Eq.(1), the photoemission matrix $M(\mathbf{k}, E, \omega)$ is dissolved as

$$M(\mathbf{k}, E, \omega) = \int d\mathbf{k}' d\mathbf{k}'' d\mathbf{k}''' d\mathbf{k}'''' \langle \tilde{\mathbf{k}} | G_2^+ | \mathbf{k}' \rangle \langle \mathbf{k}' | \Delta | \mathbf{k}'' \rangle \quad (4)$$

$$\times \langle \mathbf{k}'' | G_1^+ | \mathbf{k}''' \rangle \langle \mathbf{k}''' | \Delta^\dagger | \mathbf{k}'''' \rangle \langle \mathbf{k}'''' | G_2^- | \tilde{\mathbf{k}} \rangle,$$

where G_1 and G_2 denote the one-particle Green's functions at E and $E + \omega$, respectively, and $\Delta = \hat{\mathbf{E}} \cdot \mathbf{p}$, we would get, assuming the linear polarized photon,

$$\langle \mathbf{k}' | \Delta | \mathbf{k}'' \rangle = (\hat{\mathbf{E}} \cdot \mathbf{k}') \delta(\mathbf{k}' - \mathbf{k}''), \quad \mathbf{k} = (\mathbf{K}, k_z). \quad (5)$$

III. PHOTOEMISSION IN THE SYSTEM OF CHAINS : FOR $\text{PrBa}_2\text{Cu}_3\text{O}_7$

The low energy features in ARPES for PBCO are expected to be governed by the CuO_3 chain. In a formula unit, $R\text{Ba}_2\text{Cu}_3\text{O}_7$ (R =rare earth) has pairs of CuO_2 planes between CuO_3 chain layers. Among those compounds, for the case of $\text{PrBa}_2\text{Cu}_3\text{O}_7$, various experimental [8] and theoretical studies [9] suggests that the CuO_2 plane should not be doped, but the CuO_3 chain doped. In this study, we do not consider the undoped CuO_2 plane since its contributions will be pushed to high binding energies.

The chains are along the y -direction (b -axis). Then the formal Green's function of the system in the real space representation can be written as

$$G^\pm(\mathbf{r}, \mathbf{r}') = \sum_s \sum_{mm'} \frac{\psi_s^{mm'}(\mathbf{r}) \psi_s^{mm'*}(\mathbf{r}')}{E - \epsilon_s \pm i0^+}, \quad (6)$$

where $\psi_s^{mm'}(\mathbf{r})$ are eigenstates of the system, $\psi_s^{mm'}(\mathbf{r}) = \psi_s(y)\chi(x - c_{\parallel}m)\chi(z - c_{\perp}m')$. Here $\psi_s(y)$ is assumed to include both charge and spin degrees of freedom, while in the direction perpendicular to the chain the minimum excitation energy is assumed to be so high that $\chi(x)$ or $\chi(z)$ is taken the lowest localized one-dimensional state. Besides, we assume the overlap between the chains is very small. Then, if we rewrite Eq.(6) in a more explicit way,

$$G^\pm(\mathbf{r}, \mathbf{r}') = \bar{G}^\pm(y - y') \sum_{m=-\infty}^{\infty} \chi(x - c_{\parallel}m) \chi^*(x' - c_{\parallel}m)$$

$$\times \sum_{m'=0}^{\infty} \chi(z - c_{\perp}m' - \frac{c_{\perp}}{2}) \chi^*(z' - c_{\perp}m' - \frac{c_{\perp}}{2}), \quad (7)$$

where we have assumed that $z = 0$ is the surface and the first chain layer is positioned at $z = \frac{c_{\perp}}{2}$. $\bar{G}^\pm(y - y')$ is an ordinary single-particle Green's function in the Luttinger liquid including both charge and spin degrees of freedom. In the Luttinger model, the single-particle Green's function and its property are already well known [17]. This trivial factorization of the Luttinger Green's function is thanks to the complete suppression of the perpendicular excitation by the starting assumption. It should be also noted that, for the interchain distances, experiments give $c_a \sim c_b = c_{\parallel}$ and $c_{\perp} \sim 3c_{\parallel}$ [18].

Now we see $\langle \tilde{\mathbf{k}} | G | \mathbf{k}' \rangle$ is

$$\langle \tilde{\mathbf{k}} | G | \mathbf{k}' \rangle = \bar{G}(k_y) \delta(k_y - k'_y) \sum_{m=0}^{\infty} \tilde{\chi}^m(k_z) [\bar{\chi}^m(k'_z)]^*$$

$$\times \chi(k_x) \chi^*(k'_x) \left[\frac{1}{c_{\parallel}} \sum_{G_{\parallel}} \delta(k_x - k'_x + G_{\parallel}) \right], \quad (8)$$

where $G_{\parallel} = 2n\pi/c_{\parallel}$ is the in-plane reciprocal lattice vector due to the periodic lattice. For the explicit calculation, we propose a suitable exponential form for $\chi(x)$ (or $\chi(z)$),

$$\chi(x) = \frac{1}{\sqrt{a}} e^{-|x|/a}, \quad \chi(k_x) = \sqrt{\frac{2a}{\pi}} \frac{1}{1 + k_x^2 a^2}, \quad (9)$$

and additionally,

$$\tilde{\chi}^m(k_z) = \frac{1}{\sqrt{2\pi a}} \frac{2/a}{1/a^2 + \tilde{k}_z^2} e^{i\tilde{k}_z(c_{\perp}m + c_{\perp}/2)}$$

$$- \frac{1}{\sqrt{2\pi a}} \left[\frac{1}{1/a + i\tilde{k}_z} - \frac{1}{1/a + ik_z} \right] e^{-\frac{1}{a}(c_{\perp}m + c_{\perp}/2)},$$

$$\bar{\chi}^m(k_z) = \chi(k_z) e^{ik_z(c_{\perp}m + c_{\perp}/2)}. \quad (10)$$

Here we basically assume $c_{\parallel}, c_{\perp} \gg a$. In Eq.(10), $\tilde{\chi}^m(k_z)$ is reduced into $\bar{\chi}^m(k_z)$ when replacing \tilde{k}_z by k_z . Using Eqs.(8),(9), and (10), we get the photoemission matrix $M(\mathbf{k}, E, \omega)$, aside from irrelevant constants,

$$M(\mathbf{k}, E, \omega) = |\bar{G}_2(k_y)|^2 \bar{G}_1^+(k_y) |\chi(k_x)|^2 \quad (11)$$

$$\times \sum_m \sum_{m'} \sum_{m''} \tilde{\chi}^m(k_z) [\tilde{\chi}^{m''}(k_z)]^*$$

$$\times \int dk'_z dk''_z \sum_{G_{\parallel}} \sum_{G'_{\parallel}} |\chi(k_x + G_{\parallel})|^2 |\chi(k_x + G'_{\parallel})|^2$$

$$\times [\varepsilon_x(k_x + G_{\parallel}) + \varepsilon_y k_y + \varepsilon_z k'_z]$$

$$\times [\varepsilon_x(k_x + G'_{\parallel}) + \varepsilon_y k_y + \varepsilon_z k''_z]$$

$$\times [\bar{\chi}^m(k'_z)]^* \bar{\chi}^{m'}(k'_z) [\bar{\chi}^{m''}(k''_z)]^* \bar{\chi}^{m''}(k''_z),$$

where $\hat{\mathbf{E}} = (\varepsilon_x, \varepsilon_y, \varepsilon_z)$ and $m, m',$ and m'' run from 0 to $+\infty$. Equation (11) involves two types of summations with respect to G_{\parallel} . The summation for the reciprocal lattice vector can be done by use of

$$\sum_{G_{\parallel}} e^{iG_{\parallel}x} = c_{\parallel} \sum_{m=-\infty}^{\infty} \delta(x - c_{\parallel}m). \quad (12)$$

First, using Eq.(12), let us note and define

$$\begin{aligned} \sum_{G_{\parallel}} |\chi(k_x + G_{\parallel})|^2 &= \frac{2a}{\pi} \sum_{G_{\parallel}} \frac{1}{[1 + (k_x + G_{\parallel})^2 a^2]^2} \\ &= \frac{c_{\parallel}}{2\pi} \sum_m e^{ik_x c_{\parallel} m} [c_{\parallel} |m|/a + 1] e^{-c_{\parallel} |m|/a} \\ &\equiv \xi(k_x), \end{aligned} \quad (13)$$

and in the same way,

$$\begin{aligned} \sum_{G_{\parallel}} (k_x + G_{\parallel}) |\chi(k_x + G_{\parallel})|^2 &= \frac{2a}{\pi} \sum_{G_{\parallel}} \frac{k_x + G_{\parallel}}{[1 + (k_x + G_{\parallel})^2 a^2]^2} \\ &= -\frac{i}{2\pi} \frac{c_{\parallel}^2}{a^2} \sum_{m \neq 0} e^{ik_x c_{\parallel} m} m e^{-c_{\parallel} |m|/a} \zeta(k_x) \\ &\equiv \zeta(k_x). \end{aligned} \quad (14)$$

For the x -direction, the lattice is so infinitely periodic that m runs from $-\infty$ to $+\infty$, which should be distinguished from the z -direction. In an actual calculation of $\xi(k_x)$ and $\zeta(k_x)$, it will be enough to have the first few terms of the infinite series because we have a well-defined small expansion parameter $e^{-c_{\parallel}/a}$. For a further calculation of Eq.(11), we feel like getting a simpler form of $\tilde{\chi}^m(k_z)$ than in Eq.(10). If we think of a small damping case ($k_z \gg \Gamma$), we can simplify Eq.(10) into

$$\tilde{\chi}^m(k_z) \approx \chi(k_z) e^{-\text{Im}\tilde{k}_z(c_{\perp}m + c_{\perp}/2)} e^{ik_z(c_{\perp}m + c_{\perp}/2)}, \quad (15)$$

and $\text{Im}\tilde{k}_z \approx \Gamma/2|k_z|$. On the other hand, we can readily perform the remaining integrals for k'_x and k''_x ,

$$\begin{aligned} \int dk_z [\tilde{\chi}^m(k_z)]^* \tilde{\chi}^{m'}(k_z) &= \frac{2}{\pi a^3} \int dk_z \frac{e^{-ik_z c_{\perp}(m-m')}}{(1/a^2 + k_z^2)^2} \\ &= [c_{\perp} |m - m'|/a + 1] e^{-c_{\perp} |m - m'|/a} \\ &\equiv \bar{\xi}(m - m'), \end{aligned} \quad (16)$$

and also in the same way,

$$\begin{aligned} \int dk_z k_z [\tilde{\chi}^m(k_z)]^* \tilde{\chi}^{m'}(k_z) &= \frac{2}{\pi a^3} \int dk_z k_z \frac{e^{-ik_z c_{\perp}(m-m')}}{(1/a^2 + k_z^2)^2} \\ &= -\frac{i}{a} \frac{c_{\perp}}{a} (m - m') e^{-c_{\perp} |m - m'|/a}, \\ &\equiv \bar{\zeta}(m - m'). \end{aligned} \quad (17)$$

From Eqs.(13)-(17), we can reexpress $M(\mathbf{k}, E, \omega)$ into a form including only the summations for m 's,

$$\begin{aligned} M(\mathbf{k}, E, \omega) &= |\bar{G}_2(k_y)|^2 \bar{G}_1^+(k_y) |\chi(k_x)|^2 |\chi(k_z)|^2 e^{-\text{Im}\tilde{k}_z c_{\perp}} \\ &\times \sum_m \sum_{m'} \sum_{m''} e^{-\text{Im}\tilde{k}_z c_{\perp}(m+m'')} e^{ik_z c_{\perp}(m-m'')} \\ &\times [\varepsilon_x^2 \zeta(k_x)^2 \bar{\xi}(m - m') \bar{\xi}(m' - m'') \\ &+ \varepsilon_y^2 k_y^2 \xi(k_x)^2 \bar{\xi}(m - m') \bar{\xi}(m' - m'') \\ &+ \varepsilon_z^2 \xi(k_x)^2 \bar{\zeta}(m - m') \bar{\zeta}(m' - m'') \\ &+ 2\varepsilon_x \varepsilon_y k_y \xi(k_x) \zeta(k_x) \bar{\xi}(m - m') \bar{\xi}(m' - m'') \\ &+ \varepsilon_y \varepsilon_z k_y \xi(k_x)^2 \bar{\xi}(m - m') \bar{\zeta}(m' - m'') \\ &+ \varepsilon_y \varepsilon_z k_y \xi(k_x)^2 \bar{\zeta}(m - m') \bar{\xi}(m' - m'') \\ &+ \varepsilon_z \varepsilon_x \xi(k_x) \zeta(k_x) \bar{\xi}(m - m') \bar{\zeta}(m' - m'') \\ &+ \varepsilon_z \varepsilon_x \xi(k_x) \zeta(k_x) \bar{\zeta}(m - m') \bar{\xi}(m' - m'')]. \end{aligned} \quad (18)$$

This looks still formidable complicated summations, but we can do a systematic summation thanks to a small parameter $e^{-c_{\perp}/a}$ (or $e^{-c_{\parallel}/a}$, note $c_{\perp} \sim 3c_{\parallel}$). In order to retain up to the lowest order of $e^{-c_{\perp}/a}$, we can do a summation keeping $|m - m'| \leq 1$ and $|m' - m''| \leq 1$. This is in the end same order of approximation in $\xi(k_x)$ and $\zeta(k_x)$ up to $e^{-3c_{\parallel}/a}$. That is, we have from Eqs.(13) and

$$\begin{aligned} \xi(k_x) &\approx \frac{c_{\parallel}}{2\pi} [1 + 2 \cos(k_x c_{\parallel})(c_{\parallel}/a + 1) e^{-c_{\parallel}/a} \\ &+ 2 \cos(2k_x c_{\parallel})(2c_{\parallel}/a + 1) e^{-2c_{\parallel}/a} \\ &+ 2 \cos(3k_x c_{\parallel})(3c_{\parallel}/a + 1) e^{-3c_{\parallel}/a}], \end{aligned} \quad (19)$$

$$\begin{aligned} \zeta(k_x) &\approx \frac{1}{\pi} \frac{c_{\parallel}^2}{a^2} [\sin(k_x c_{\parallel}) e^{-c_{\parallel}/a} + 2 \sin(2k_x c_{\parallel}) e^{-2c_{\parallel}/a} \\ &+ 3 \sin(3k_x c_{\parallel}) e^{-3c_{\parallel}/a}]. \end{aligned} \quad (20)$$

We then have three kinds of summations in Eq.(18); we define those as $\alpha(k_z)$, $\beta(k_z)$, and $\gamma(k_z)$.

$$\begin{aligned} \alpha(k_z) &\times (1 - e^{-2\text{Im}\tilde{k}_z c_{\perp}}) \\ &\equiv \sum_m \sum_{m'} \sum_{m''} e^{-\text{Im}\tilde{k}_z c_{\perp}(m+m'')} e^{ik_z c_{\perp}(m-m'')} \\ &\times \bar{\xi}(m - m') \bar{\xi}(m' - m'') (1 - e^{-2\text{Im}\tilde{k}_z c_{\perp}}) \\ &\approx 1 + (c_{\perp}/a + 1)^2 e^{-2c_{\perp}/a} (1 + e^{-2\text{Im}\tilde{k}_z c_{\perp}}) \\ &+ 4 \cos(k_z c_{\perp})(c_{\perp}/a + 1) e^{-c_{\perp}/a} e^{-\text{Im}\tilde{k}_z c_{\perp}} \\ &+ 2 \cos(2k_z c_{\perp})(c_{\perp}/a + 1)^2 e^{-2c_{\perp}/a} e^{-2\text{Im}\tilde{k}_z c_{\perp}}, \end{aligned} \quad (21)$$

$$\begin{aligned} \beta(k_z) &\times (1 - e^{-2\text{Im}\tilde{k}_z c_{\perp}}) \\ &\equiv \sum_m \sum_{m'} \sum_{m''} e^{-\text{Im}\tilde{k}_z c_{\perp}(m+m'')} e^{ik_z c_{\perp}(m-m'')} \\ &\times \bar{\zeta}(m - m') \bar{\zeta}(m' - m'') (1 - e^{-2\text{Im}\tilde{k}_z c_{\perp}}) \\ &\approx \frac{1}{a^2} (c_{\perp}/a)^2 e^{-2c_{\perp}/a} (1 + e^{-2\text{Im}\tilde{k}_z c_{\perp}}) \\ &- \frac{2}{a^2} \cos(2k_z c_{\perp})(c_{\perp}/a)^2 e^{-2c_{\perp}/a} e^{-2\text{Im}\tilde{k}_z c_{\perp}}, \end{aligned} \quad (22)$$

$$\begin{aligned}
& \gamma(k_z) \times (1 - e^{-2\text{Im}\bar{k}_z c_\perp}) \\
& \equiv \text{Re} \sum_m \sum_{m'} \sum_{m''} e^{-\text{Im}\bar{k}_z c_\perp (m+m'')} e^{ik_z c_\perp (m-m'')} \\
& \quad \times \bar{\xi}(m-m') \bar{\zeta}(m'-m'') (1 - e^{-2\text{Im}\bar{k}_z c_\perp}) \\
& \approx \frac{2}{a} \sin(2k_z c_\perp) (c_\perp/a + 1) (c_\perp/a) e^{-2c_\perp/a} e^{-2\text{Im}\bar{k}_z c_\perp} \\
& \quad + \frac{2}{a} \sin(k_z c_\perp) (c_\perp/a) e^{-c_\perp/a} e^{-\text{Im}\bar{k}_z c_\perp}. \tag{23}
\end{aligned}$$

Now, all the summation parts of Eq.(18) are found to be real as it should be. Therefore, the photoemission intensity $I(\mathbf{k}, E, \omega)$ will be proportional to $[-\frac{1}{\pi} \text{Im}\bar{G}_1^+(k_y)]$. Another factor related to the chain degree of freedom is $|\bar{G}_2(k_y)|^2 (= [\text{Re}\bar{G}_2(k_y)]^2 + [\text{Im}\bar{G}_2(k_y)]^2)$, which gives the structure in the final states. Since $E + \omega \gg E$, we can assume the final states form a structureless smooth continuum. We do not have to make the problem difficult unnecessarily.

Then we can find an analytic solution of the problem. The photoemission intensity $I(\mathbf{k}, E, \omega)$ is

$$\begin{aligned}
I(\mathbf{k}, E, \omega) \propto & \left[-\frac{1}{\pi} \text{Im}\bar{G}_1^+(k_y) \right] |\chi(k_x)|^2 |\chi(k_z)|^2 e^{-\text{Im}\bar{k}_z c_\perp} \\
& \times [\varepsilon_x^2 \zeta(k_x)^2 \alpha(k_z) + \varepsilon_y^2 k_y^2 \xi(k_x)^2 \alpha(k_z) \\
& + \varepsilon_z^2 \xi(k_x)^2 \beta(k_z) + 2\varepsilon_x \varepsilon_y k_y \xi(k_x) \zeta(k_x) \alpha(k_z) \\
& + 2\varepsilon_y \varepsilon_z k_y \xi(k_x)^2 \gamma(k_z) + 2\varepsilon_z \varepsilon_x \xi(k_x) \zeta(k_x) \gamma(k_z)], \tag{24}
\end{aligned}$$

where we note $k_z = \sqrt{2(E + \omega) - k_x^2 - k_y^2}$.

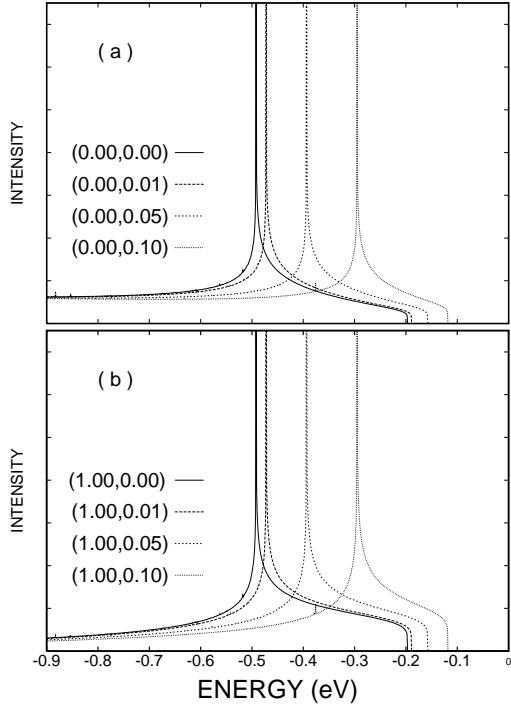


FIG. 1. Photoemission spectra in the chain direction ($\parallel k_y$) for $\hat{\mathbf{E}} \parallel xz$. It is seen that the strong k_x -dependencies are inherent in the spectra. In (a), the spectra along $(0, 0) \rightarrow (0, k_y)$ and in (b), the spectra along $(1, 0) \rightarrow (1, k_y)$ are provided.

For an actual calculation and its comparison with experiment, the reference experiment should be Mizokawa *et al.*'s [10]. In the experiment, the Fermi energy (the width of occupied band) is estimated about 0.2 eV and the Fermi wave vector $k_f = 0.25 \frac{\pi}{c_\parallel}$. In theory, the Fermi energy ϵ_f is given by the linear dispersion within Luttinger model such that $\epsilon_f = v_f k_f$. In the spectral function of Luttinger model, i.e., in $[-\frac{1}{\pi} \text{Im}\bar{G}_1^+(k_y)]$, we see two features corresponding to the collective charge (holon) and spin (spinon) excitations.

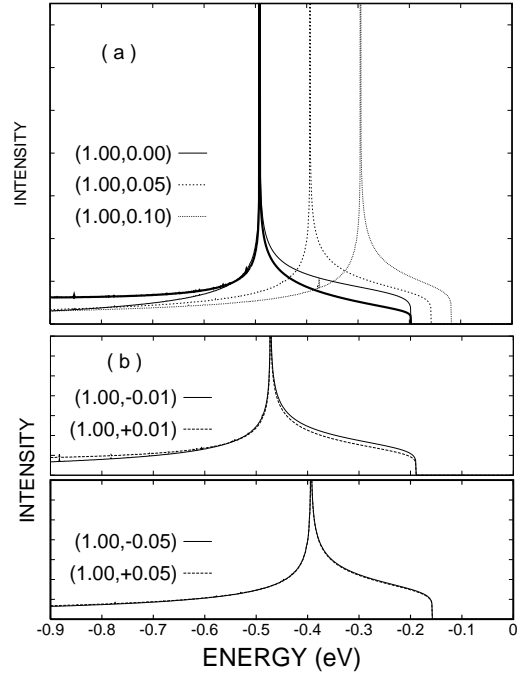


FIG. 2. Photoemission spectra for $\hat{\mathbf{E}} \parallel yz$, where \mathbf{E} has a component parallel to the chain. In (a), the spectra along $(1, 0) \rightarrow (1, k_y)$ and in (b), the spectra along $(1, -k_y) \rightarrow (1, k_y)$ are provided. The spectra at $(0, 0)$ are also given in (a) as a thick solid line.

The character of features generally rely on the interaction property through the singularity index α . If $\alpha < 1/2$, there happens a diverging sharp peak at the spinon onset, but if $\alpha > 1/2$, a converging threshold. $\alpha \sim 0.65$ is estimated from optical study of $\text{PrBa}_2\text{Cu}_4\text{O}_8$ [19]. Here we employ this value for PBCO. The charge contribution is peaked at $-v_f^c(k_f - k_y)$ and the spin excitation at $-v_f(k_f - k_y)$, where we are having the spin-independent interaction in mind. v_f^c for the holon is taken a little

larger as $v_f^c/v_f \sim 2.5$ to be consistent with qualitative behaviors of experiment [20]. The natural energy unit in theory is $(\pi/c_{\parallel})^2$, whose value is about 5.2 eV from $c_{\parallel} \sim 3.8\text{\AA}$. From the dispersion, we put $\epsilon_f = v_f k_f$, $v_f \sim 0.15 \frac{\pi}{c_{\parallel}}$ and $\epsilon_f \sim 0.038(\pi/c_{\parallel})^2$. The used photon energy in the experiment is 29 eV and $\sim 145\epsilon_f$, from which we take in the calculation the photon energy $\omega \sim 145\epsilon_f \sim 5.5(\pi/c_{\parallel})^2$. However the calculation is found quite robust with the parameters. The next thing to be considered is a constant damping parameter Γ . We take $\Gamma = 0.1(\pi/c_{\parallel})^2$. This corresponds to the mean free path $\lambda \sim \frac{v}{2\Gamma} \sim \frac{\sqrt{2}\omega}{2\Gamma} \sim 5.3c_{\parallel}$. Thinking of $c_{\perp} \sim 3c_{\parallel}$ and that the first layer is at $\frac{c_{\perp}}{2}$, λ amounts to governing one or two layers. This looks more or less acceptable. In the calculation, we take $c_{\parallel}/a = 2.5$, i.e., $c_{\perp}/a = 7.5$.

Due to the one-dimensionality itself, the chain system is expected to show a strong polarization dependency. In fact, this is a useful clue in finding one-dimensional character submerged in two-dimensional properties. In Fig.1, the photoemission spectra for the photon polarization $\hat{\mathbf{E}} \parallel xz$, more explicitly $\hat{\mathbf{E}} = (\frac{1}{\sqrt{2}}, 0, \frac{1}{\sqrt{2}})$, are shown. In the figure, we attribute the high binding energy structure, the sharp peak dispersing between ~ -0.5 eV and ~ -0.3 eV to the charge excitation (holon) and the low binding energy structure, the threshold at ~ -0.2 eV to the spin excitation (spinon). When $k_x = 0$ (Fig.1(a)), the spinon part is highly suppressed, while when $k_x = 1$ (Fig.1(b)), the spinon part is much enhanced. In the experiment [10], for $k_x = 0$ or small k_x 's, the spinon branch has not been observed and for $k_x \sim 1$, the spinon has been so enhanced that it can be observed. Therefore, these theoretical and experimental observations has been found in good agreement and consistent with each other. It need to be noticed that PBCO is an insulator due to a charge density wave (CDW) gap opening at $k_y \sim 0.25 \frac{\pi}{c_{\parallel}}$, while the Luttinger model signifies in principle a metallic system. In the study, we provide the results for k_y 's away from k_f because the spin-charge separation is seen only for small $|k_y|$ and disappears for $k_y \sim k_f$. Further agreement can be found for $\hat{\mathbf{E}} \parallel yz$, actually $\hat{\mathbf{E}} = (0, \frac{1}{\sqrt{2}}, \frac{1}{\sqrt{2}})$ in Fig.2. In the experiment [10], the spectra have been suppressed for small k_x , but comparable to the configuration of $\hat{\mathbf{E}} \parallel xz$ when $k_x \sim 1$. This is well understood from our theory as shown in Fig.2(a). Comparison of the simplest cases (1,0) and (0,0) for both polarizations (Figs.1 and 2) shows the k_x (perpendicular momentum)-dependency clearly, whose behaviors are determined by the third term in Eq.(24), $\xi(k_x)^2\beta(k_z)$. It is shown in Fig.3 that $\beta(k_z)$ could reinforce or suppress the spinon parts depending on the momentum perpendicular to the chain, i.e., k_x . In the configuration of $\hat{\mathbf{E}} \parallel yz$, the \mathbf{E} has a component parallel to the chain, so the symmetry of the system, when $k_y \leftrightarrow -k_y$, breaks. Indeed, the phase space showing the stronger spinon contribution is along $(1, 0) \rightarrow (1, -k_y)$ rather than $(1, 0) \rightarrow (1, k_y)$ (for $k_y > 0$). Figure 2(b) shows this asymmetry also suc-

cessfully at least in a qualitative picture. In the calculations, the asymmetry comes from $k_y\xi(k_x)^2\gamma(k_z)$ in Eq.(24). The obtained asymmetry is in fact weaker than the experiment and rapidly fades away as $|k_y|$ increases. In the figures, the absolute intensity variations with respect to several \mathbf{k} 's would not be very reliable here because of many simplifications. Nevertheless, our model of the 1/4-filled three-dimensional chain array is found to explain very well the one-dimensional behaviors, especially the relative charge and spin intensities, reflected in the recent ARPES data.

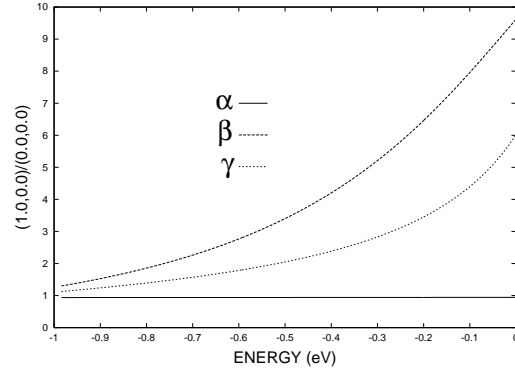


FIG. 3. The ratios of $\alpha(k_z)$, $\beta(k_z)$, and $\gamma(k_z)$ for two simple cases (1,0) and (0,0) are given, i.e., $\alpha = \frac{\alpha(k_z, k_x=1, k_y=0)}{\alpha(k_z, k_x=0, k_y=0)}$ and same as for β and γ .

Another one-dimensional insulator SrCuO₂ also has Cu-O chains. Even if there is a finite interchain coupling, it is an order of magnitude weaker than the intra-chain coupling, which makes SrCuO₂ a one-dimensional compound. Aside from several details, we find that the present calculations should be relevant to the SrCuO₂ system as well. In fact, the ARPES experiment on SrCuO₂ shows that the qualitative behaviors are very similar to the PBCO case (See Figs. 4 and 5 in Ref. [13]) in that the spinon bands are more apparent in the case of large (~ 1) momentum perpendicular to the chain.

IV. PHOTOEMISSION IN THE SYSTEM OF CHAINS : FOR $\text{La}_{2-x-y}\text{Nd}_y\text{Sr}_x\text{CuO}_4$

In the so called stripe phase, there happens the one-dimensional spin-charge modulations in the two-dimensional CuO₂ planes. The stripe phase has attracted much attention in connection with its implication to high T_C superconductivity since it was proposed from neutron scattering in Nd-substituted $\text{La}_{2-x-y}\text{Nd}_y\text{Sr}_x\text{CuO}_4$ (Nd-LSCO) [12]. It has been also reported that the charge transport in Nd-LSCO is observed to be one-dimensional, also consistent with the static stripe phase formation [21]. Similar stripe signatures are observed in $\text{La}_{2-x}\text{Sr}_x\text{CuO}_4$ (LSCO) [22] despite of their dynamical natures, while the stripe phase in Nd-LSCO is considered static. In this section, we extend the model described in the pre-

vious section and apply to the Nd-LSCO system. It is one of the key issues whether the stripe phase is intrinsically metallic or insulating. Here, however, our study will proceed based on the simple assumption of metallic one-dimensional system. As assumed before, our model has completely suppressed the interchain (interstripe) interaction and out-of-chain excitation and may be more suitable for describing the static stripe phase. So Nd-LSCO will be preferred in our theory. Nd-LSCO has characteristic stripe (one-dimensional) phases, where the stripes in adjacent planes are rotated by $\frac{\pi}{2}$, whose schematic sketch is given in Fig.4. It should be noted, however, that the ARPES study of LSCO with dynamical stripes shows similar characteristics such as one-dimension-like low energy electronic structure and the suppression of nodal states [23]. Therefore, the studies of static stripes would help to understand the dynamical stripes, too.

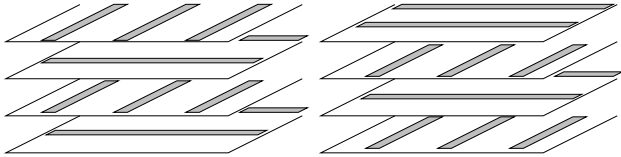


FIG. 4. Schematic view of the static stripe phase observed in Nd-LSCO. In the study, the stripe would be modeled as a linear charged chain. In an actual experimental situation, both configurations have been equally mixed.

In the study, we are bearing $\text{La}_{1.28}\text{Nd}_{0.6}\text{Sr}_{0.12}\text{CuO}_4$ in our mind as being the reference compound, available in the recent ARPES experiment [14]. In this doping, each charged stripe is separated by three undoped stripes, so the system has a periodicity of $4l$ (l is the lattice constant in the in-plane direction), whereas the stripe itself is $1/4$ filled. Then the in-plane interchain (between charged stripes) distance c_{\parallel} would be $c_{\parallel} = 4l$ and the out-of-plane distance would be $c_{\perp} \sim 2l$. Here, the wave vector unit should be π/l . In the unit, the Fermi wave vector is $1/4$. In principle, the starting point is exactly same as in PBCO, in the previous section III except that each stripe is assumed a Fermi liquid rather than a Tomonaga-Luttinger liquid. For describing the stripes perpendicularly crossed layer by layer, we write the Green's function of the system

$$G_i(\mathbf{r}, \mathbf{r}') = \bar{G}_i(y - y') \sum_{m=-\infty}^{\infty} \chi(x - c_{\parallel}m) \chi^*(x' - c_{\parallel}m) \quad (25)$$

$$\times \sum_{m'=0}^{\infty} \chi(z - 2c_{\perp}m' - \frac{c_{\perp}}{2}) \chi^*(z' - 2c_{\perp}m' - \frac{c_{\perp}}{2})$$

$$+ \bar{G}_i(x - x') \sum_{m=-\infty}^{\infty} \chi(y - c_{\parallel}m) \chi^*(y' - c_{\parallel}m)$$

$$\times \sum_{m'=0}^{\infty} \chi(z - 2c_{\perp}m' - \frac{3c_{\perp}}{2}) \chi^*(z' - 2c_{\perp}m' - \frac{3c_{\perp}}{2})$$

$$= G_{i1}(\mathbf{r}, \mathbf{r}') + G_{i2}(\mathbf{r}, \mathbf{r}'), \quad i = 1, 2$$

where $i = 1, 2$ denote the Green function at E and $E + \omega$, respectively. The surface is assumed to be at $z = 0$. The Green's function matrix element $\langle \tilde{\mathbf{k}} | G_i | \mathbf{k}' \rangle$ is

$$\langle \tilde{\mathbf{k}} | G_i | \mathbf{k}' \rangle = \bar{G}_i(k_y) \delta(k_y - k'_y)$$

$$\times \chi(k_x) \chi^*(k'_x) \left[\frac{1}{c_{\parallel}} \sum_{G_{\parallel}} \delta(k_x - k'_x + G_{\parallel}) \right]$$

$$\times \sum_{m=0}^{\infty} \tilde{\chi}^m(k_z) [\bar{\chi}^m(k'_z)]^*$$

$$+ \bar{G}_i(k_x) \delta(k_x - k'_x)$$

$$\times \chi(k_y) \chi^*(k'_y) \left[\frac{1}{c_{\parallel}} \sum_{G_{\parallel}} \delta(k_y - k'_y + G_{\parallel}) \right]$$

$$\times \sum_{m=0}^{\infty} \tilde{\chi}^{m+\frac{1}{2}}(k_z) [\bar{\chi}^{m+\frac{1}{2}}(k'_z)]^*$$

$$= \langle \tilde{\mathbf{k}} | G_{i1} | \mathbf{k}' \rangle + \langle \tilde{\mathbf{k}} | G_{i2} | \mathbf{k}' \rangle, \quad (26)$$

where $G_{\parallel} = 2n\pi/c_{\parallel}$ is the reciprocal lattice vector for an in-plane direction. Following the same line of approximation as in the previous PBCO case, we note

$$\bar{\chi}^m(k_z) = \frac{1}{\sqrt{2\pi a}} \frac{2/a}{1/a^2 + k_z^2} e^{ik_z(2c_{\perp}m + c_{\perp}/2)},$$

$$\tilde{\chi}^m(k_z) = \frac{1}{\sqrt{2\pi a}} \frac{2/a}{1/a^2 + k_z^2} e^{ik_z(2c_{\perp}m + c_{\perp}/2)}. \quad (27)$$

Then we see the photoemission intensity $I(\mathbf{k}, E, \omega)$ is expressed as (adopting the simplified notation), for $\Delta = \hat{E} \cdot \mathbf{p}$,

$$I(\mathbf{k}, E, \omega) \propto G_{21}^+ \Delta G_{11}^+ \Delta G_{21}^- + G_{22}^+ \Delta G_{12}^+ \Delta G_{22}^-$$

$$+ G_{22}^+ \Delta G_{11}^+ \Delta G_{22}^- + G_{21}^+ \Delta G_{12}^+ \Delta G_{21}^-$$

$$+ G_{21}^+ \Delta G_{11}^+ \Delta G_{22}^- + G_{22}^+ \Delta G_{11}^+ \Delta G_{21}^-$$

$$+ G_{21}^+ \Delta G_{12}^+ \Delta G_{22}^- + G_{22}^+ \Delta G_{12}^+ \Delta G_{21}^-, \quad (28)$$

where we readily recognize only the first two terms ($G_{21}^+ \Delta G_{11}^+ \Delta G_{21}^-$ and $G_{22}^+ \Delta G_{12}^+ \Delta G_{22}^-$) are the direct term for each y - and x -directed chain set with the perpendicular interchain distance $2c_{\perp}$, while the others are given by the complex interferences of two perpendicular sets. The calculation can be done in the same way as in the section III, but its algebra is quite long and tedious. The final expression has a slight asymmetry in interchanging x - and y -coordinates depending on which set is the first layer. Thanks to the remaining symmetries in Eq.(28), nevertheless, it will be enough to calculate the half of terms and the other half could be obtained by interchanging $k_x \leftrightarrow k_y$ and $\varepsilon_x \leftrightarrow \varepsilon_y$ if only one account for some damping terms.

In Eq.(28), $G_{21}^+ \Delta G_{11}^+ \Delta G_{21}^-$ is exactly same calculation as in Eq.(24) except for a little changes like $c_\perp \rightarrow 2c_\perp$ in $\alpha(k_z)$, $\beta(k_z)$, and $\gamma(k_z)$. Here for a later use, we redefine $\alpha(k_z)$, $\beta(k_z)$, $\gamma(k_z)$, $\bar{\xi}(m)$, and $\bar{\zeta}(m)$ by putting $c_\perp \rightarrow 2c_\perp$. For $G_{22}^+ \Delta G_{11}^+ \Delta G_{22}^-$ in Eq.(28), we have the expression, apart from irrelevant constants,

$$\begin{aligned}
& G_{22}^+ \Delta G_{11}^+ \Delta G_{22}^- \quad (29) \\
&= \left[-\frac{1}{\pi} \text{Im} \bar{G}_1^+(k_y) \right] |\chi(k_x)|^2 |\chi(k_y)|^2 |\chi(k_z)|^2 e^{-3\text{Im} \bar{k}_z c_\perp} \\
&\times \sum_m \sum_{m'} \sum_{m''} e^{-2\text{Im} \bar{k}_z c_\perp (m+m'')} e^{i2k_z c_\perp (m-m'')} \\
&\times \left[\varepsilon_x^2 k_x^2 \xi(k_y) \bar{\xi}(m-m'+\frac{1}{2}) \bar{\xi}(m'-m''-\frac{1}{2}) \right. \\
&+ \varepsilon_y^2 \eta(k_y) \bar{\xi}(m-m'+\frac{1}{2}) \bar{\xi}(m'-m''-\frac{1}{2}) \\
&+ \varepsilon_z^2 \xi(k_y) \bar{\zeta}(m-m'+\frac{1}{2}) \bar{\zeta}(m'-m''-\frac{1}{2}) \\
&+ 2\varepsilon_x \varepsilon_y k_x \zeta(k_y) \bar{\xi}(m-m'+\frac{1}{2}) \bar{\xi}(m'-m''-\frac{1}{2}) \\
&+ \varepsilon_y \varepsilon_z \zeta(k_y) \bar{\xi}(m-m'+\frac{1}{2}) \bar{\zeta}(m'-m''-\frac{1}{2}) \\
&+ \varepsilon_y \varepsilon_z \zeta(k_y) \bar{\zeta}(m-m'+\frac{1}{2}) \bar{\xi}(m'-m''-\frac{1}{2}) \\
&+ \varepsilon_z \varepsilon_x k_x \xi(k_y) \bar{\zeta}(m-m'+\frac{1}{2}) \bar{\xi}(m'-m''-\frac{1}{2}) \\
&\left. + \varepsilon_z \varepsilon_x k_x \xi(k_y) \bar{\xi}(m-m'+\frac{1}{2}) \bar{\zeta}(m'-m''-\frac{1}{2}) \right],
\end{aligned}$$

where $\eta(k)$ is another G_{\parallel} -summation not appeared in section III,

$$\begin{aligned}
& \sum_{G_{\parallel}} (k+G_{\parallel})^2 |\chi(k+G_{\parallel})|^2 \\
&= \frac{1}{2\pi a} \frac{c_{\parallel}}{a} \sum_m e^{ikc_{\parallel} m} [-c_{\parallel} |m|/a + 1] e^{-c_{\parallel} |m|/a} \\
&\approx \frac{1}{2\pi a} \frac{c_{\parallel}}{a} [1 - 2 \cos(kc_{\parallel}) (c_{\parallel}/a - 1) e^{-c_{\parallel}/a} \\
&\quad - 2 \cos(2kc_{\parallel}) (2c_{\parallel}/a - 1) e^{-2c_{\parallel}/a}] \\
&\equiv \eta(k), \quad (30)
\end{aligned}$$

and the other sophisticated summations for m , m' , and m'' (all m 's > 0) can be managed by considering the small parameter $e^{-c_\perp/a}$,

$$\begin{aligned}
\bar{\alpha}(k_z) &\equiv \sum_m \sum_{m'} \sum_{m''} e^{-2\text{Im} \bar{k}_z c_\perp (m+m'')} e^{i2k_z c_\perp (m-m'')} \\
&\times \bar{\xi}(m-m' \pm \frac{1}{2}) \bar{\xi}(m'-m'' \mp \frac{1}{2}) \\
&\approx 2(c_\perp/a + 1)^2 [1 + \cos(2k_z c_\perp)] e^{-2\text{Im} \bar{k}_z c_\perp} e^{-2c_\perp/a} \\
&\times \sum_{m=0}^{\infty} e^{-4\text{Im} \bar{k}_z c_\perp m}, \quad (31)
\end{aligned}$$

$$\bar{\beta}(k_z) \equiv \sum_m \sum_{m'} \sum_{m''} e^{-2\text{Im} \bar{k}_z c_\perp (m+m'')} e^{i2k_z c_\perp (m-m'')}$$

$$\begin{aligned}
& \times \bar{\zeta}(m-m' \pm \frac{1}{2}) \bar{\zeta}(m'-m'' \mp \frac{1}{2}) \\
&\approx \frac{2}{a^2} \frac{c_\perp^2}{a^2} [1 - \cos(2k_z c_\perp)] e^{-2\text{Im} \bar{k}_z c_\perp} e^{-2c_\perp/a} \\
&\times \sum_{m=0}^{\infty} e^{-4\text{Im} \bar{k}_z c_\perp m}, \quad (32)
\end{aligned}$$

$$\begin{aligned}
\bar{\gamma}(k_z) &\equiv \sum_m \sum_{m'} \sum_{m''} e^{-2\text{Im} \bar{k}_z c_\perp (m+m'')} e^{i2k_z c_\perp (m-m'')} \\
&\times \bar{\xi}(m-m' \pm \frac{1}{2}) \bar{\zeta}(m'-m'' \mp \frac{1}{2}) \quad (33)
\end{aligned}$$

$$\begin{aligned}
&= \sum_m \sum_{m'} \sum_{m''} e^{-2\text{Im} \bar{k}_z c_\perp (m+m'')} e^{i2k_z c_\perp (m-m'')} \\
&\times \bar{\zeta}(m-m' \pm \frac{1}{2}) \bar{\xi}(m'-m'' \mp \frac{1}{2}) \quad (34) \\
&\approx \frac{2}{a} \sin(2k_z c_\perp) (c_\perp/a) (c_\perp/a + 1) e^{-2c_\perp/a} e^{-2\text{Im} \bar{k}_z c_\perp} \\
&\times \sum_{m=0}^{\infty} e^{-4\text{Im} \bar{k}_z c_\perp m}. \quad (35)
\end{aligned}$$

The calculated $\bar{\alpha}(k_z)$, $\bar{\beta}(k_z)$, and $\bar{\gamma}(k_z)$ are correct to up to $e^{-3c_\perp/a}$. Then $G_{22}^+ \Delta G_{11}^+ \Delta G_{22}^-$ is written down

$$\begin{aligned}
& G_{22}^+ \Delta G_{11}^+ \Delta G_{22}^- \\
&= \left[-\frac{1}{\pi} \text{Im} \bar{G}_1^+(k_y) \right] |\chi(k_x)|^2 |\chi(k_y)|^2 |\chi(k_z)|^2 e^{-3\text{Im} \bar{k}_z c} \\
&\times \left[\varepsilon_x^2 k_x^2 \xi(k_y) \bar{\alpha}(k_z) + \varepsilon_y^2 \eta(k_y) \bar{\alpha}(k_z) \right. \\
&+ \varepsilon_z^2 \xi(k_y) \bar{\beta}(k_z) + 2\varepsilon_x \varepsilon_y k_x \zeta(k_y) \bar{\alpha}(k_z) \\
&\left. + 2\varepsilon_y \varepsilon_z \zeta(k_y) \bar{\gamma}(k_z) + 2\varepsilon_z \varepsilon_x k_x \xi(k_y) \bar{\gamma}(k_z) \right]. \quad (36)
\end{aligned}$$

In the calculations of $G_{21}^+ \Delta G_{11}^+ \Delta G_{21}^-$ and $G_{22}^+ \Delta G_{11}^+ \Delta G_{22}^-$, we have neglected $|\bar{G}_2(k_y)|^2$ (for the latter, $|\bar{G}_2(k_x)|^2$) based on assuming that the final state distribution may be structureless and smooth from $E + \omega \gg E$. Next we go to the evaluation of $G_{21}^+ \Delta G_{11}^+ \Delta G_{22}^- + G_{22}^+ \Delta G_{11}^+ \Delta G_{21}^-$. Here we need a more drastic assumption on behaviors of $\bar{G}_2(k_y)$, i.e., $\text{Im} \bar{G}_2(k_y) \approx 0$. Thus we assume $\bar{G}_2^+(k_y) \bar{G}_2^-(k_x)$ or $\bar{G}_2^+(k_x) \bar{G}_2^-(k_y)$ could be also taken just as a positive constant and further $|\bar{G}_2(k_y)|^2 \approx |\bar{G}_2(k_x)|^2 \approx \bar{G}_2^+(k_y) \bar{G}_2^-(k_x) \approx \bar{G}_2^+(k_x) \bar{G}_2^-(k_y)$. Then $G_{21}^+ \Delta G_{11}^+ \Delta G_{22}^-$ is

$$\begin{aligned}
& G_{21}^+ \Delta G_{11}^+ \Delta G_{22}^- \\
&= \left[-\frac{1}{\pi} \text{Im} \bar{G}_1^+(k_y) \right] |\chi(k_x)|^2 |\chi(k_y)|^2 |\chi(k_z)|^2 e^{-2\text{Im} \bar{k}_z c_\perp} \\
&\times \sum_m \sum_{m'} \sum_{m''} e^{-2\text{Im} \bar{k}_z c_\perp (m+m'')} e^{i2k_z c_\perp [m-m''-\frac{1}{2}]} \\
&\times \left[\varepsilon_x^2 k_x \zeta(k_x) \bar{\xi}(m-m') \bar{\xi}(m'-m''-\frac{1}{2}) \right. \\
&\left. + \varepsilon_y^2 k_y^2 \xi(k_x) \bar{\xi}(m-m') \bar{\xi}(m'-m''-\frac{1}{2}) \right]
\end{aligned}$$

$$\begin{aligned}
& +\varepsilon_z^2 \xi(k_x) \bar{\zeta}(m-m') \bar{\zeta}(m'-m''-\frac{1}{2}) \\
& +\varepsilon_x \varepsilon_y k_y \zeta(k_x) \bar{\xi}(m-m') \bar{\xi}(m'-m''-\frac{1}{2}) \\
& +\varepsilon_x \varepsilon_y k_x k_y \xi(k_x) \bar{\xi}(m-m') \bar{\xi}(m'-m''-\frac{1}{2}) \\
& +\varepsilon_y \varepsilon_z k_y \xi(k_x) \bar{\xi}(m-m') \bar{\zeta}(m'-m''-\frac{1}{2}) \\
& +\varepsilon_y \varepsilon_z k_y \xi(k_x) \bar{\zeta}(m-m') \bar{\xi}(m'-m''-\frac{1}{2}) \\
& +\varepsilon_z \varepsilon_x k_x \xi(k_x) \bar{\zeta}(m-m') \bar{\xi}(m'-m''-\frac{1}{2}) \\
& +\varepsilon_z \varepsilon_x \zeta(k_x) \bar{\xi}(m-m') \bar{\zeta}(m'-m''-\frac{1}{2})], \quad (37)
\end{aligned}$$

and $G_{22}^+ \Delta G_{11}^+ \Delta G_{21}^-$ is also similarly

$$\begin{aligned}
& G_{22}^+ \Delta G_{11}^+ \Delta G_{21}^- \\
& = \left[-\frac{1}{\pi} \text{Im} \bar{G}_1^+(k_y) \right] |\chi(k_x)|^2 |\chi(k_y)|^2 |\chi(k_z)|^2 e^{-2\text{Im} \bar{k}_z c_\perp} \\
& \times \sum_m \sum_{m'} \sum_{m''} e^{-2\text{Im} \bar{k}_z c_\perp (m+m'')} e^{i2k_z c_\perp [m-m''+\frac{1}{2}]} \\
& \times [\varepsilon_x^2 k_x \zeta(k_x) \bar{\xi}(m-m'+\frac{1}{2}) \bar{\xi}(m'-m'') \\
& +\varepsilon_y^2 k_y^2 \xi(k_x) \bar{\xi}(m-m'+\frac{1}{2}) \bar{\xi}(m'-m'') \\
& +\varepsilon_z^2 \xi(k_x) \bar{\zeta}(m-m'+\frac{1}{2}) \bar{\zeta}(m'-m'') \\
& +\varepsilon_x \varepsilon_y k_y \zeta(k_x) \bar{\xi}(m-m'+\frac{1}{2}) \bar{\xi}(m'-m'') \\
& +\varepsilon_x \varepsilon_y k_x k_y \xi(k_x) \bar{\xi}(m-m'+\frac{1}{2}) \bar{\xi}(m'-m'') \\
& +\varepsilon_y \varepsilon_z k_y \xi(k_x) \bar{\xi}(m-m'+\frac{1}{2}) \bar{\zeta}(m'-m'') \\
& +\varepsilon_y \varepsilon_z k_y \xi(k_x) \bar{\zeta}(m-m'+\frac{1}{2}) \bar{\xi}(m'-m'') \\
& +\varepsilon_z \varepsilon_x k_x \xi(k_x) \bar{\xi}(m-m'+\frac{1}{2}) \bar{\zeta}(m'-m'') \\
& +\varepsilon_z \varepsilon_x \zeta(k_x) \bar{\zeta}(m-m'+\frac{1}{2}) \bar{\xi}(m'-m'')]. \quad (38)
\end{aligned}$$

We can also define $\tilde{\alpha}(k_z)$, $\tilde{\beta}(k_z)$, $\tilde{\gamma}_1(k_z)$, and $\tilde{\gamma}_1(k_z)$ as the summations for m 's relevant in Eqs.(37) and (38);

$$\begin{aligned}
\tilde{\alpha}(k_z) & \equiv \text{Re} \sum_m \sum_{m'} \sum_{m''} e^{-2\text{Im} \bar{k}_z c_\perp (m+m'')} e^{i2k_z c_\perp (m-m''-\frac{1}{2})} \\
& \times \bar{\xi}(m-m') \bar{\xi}(m'-m''-\frac{1}{2}) \\
& \approx \cos(k_z c_\perp) (c_\perp/a+1) [1+(2c_\perp/a+1)e^{-2c_\perp/a}] \\
& \times e^{-c_\perp/a} (1+e^{-2\text{Im} \bar{k}_z c_\perp}) \sum_{m=0}^{\infty} e^{-4\text{Im} \bar{k}_z c_\perp m} \\
& + \cos(3k_z c_\perp) (2c_\perp/a+1) (c_\perp/a+1) e^{-2\text{Im} \bar{k}_z c_\perp} \\
& \times e^{-3c_\perp/a} (1+e^{-2\text{Im} \bar{k}_z c_\perp}) \sum_{m=0}^{\infty} e^{-4\text{Im} \bar{k}_z c_\perp m}, \quad (39)
\end{aligned}$$

$$\begin{aligned}
\tilde{\beta}(k_z) & \equiv \text{Re} \sum_m \sum_{m'} \sum_{m''} e^{-2\text{Im} \bar{k}_z c_\perp (m+m'')} e^{i2k_z c_\perp (m-m''-\frac{1}{2})} \\
& \times \bar{\zeta}(m-m') \bar{\zeta}(m'-m''-\frac{1}{2}) \\
& \approx \frac{2}{a^2} \frac{c_\perp^2}{a^2} [\cos(k_z c_\perp) - \cos(3k_z c_\perp)] e^{-2\text{Im} \bar{k}_z c_\perp} \\
& \times e^{-3c_\perp/a} (1+e^{-2\text{Im} \bar{k}_z c_\perp}) \sum_{m=0}^{\infty} e^{-4\text{Im} \bar{k}_z c_\perp m}, \quad (40)
\end{aligned}$$

$$\begin{aligned}
\tilde{\gamma}_1(k_z) & \equiv \text{Re} \sum_m \sum_{m'} \sum_{m''} e^{-2\text{Im} \bar{k}_z c_\perp (m+m'')} e^{i2k_z c_\perp (m-m''-\frac{1}{2})} \\
& \times \bar{\xi}(m-m') \bar{\zeta}(m'-m''-\frac{1}{2}) \\
& \approx \frac{1}{a} \frac{c_\perp}{a} \sin(k_z c_\perp) e^{-c_\perp/a} [1-(2c_\perp/a+1)e^{-2c_\perp/a}] \\
& \times (1+e^{-2\text{Im} \bar{k}_z c_\perp}) \sum_{m=0}^{\infty} e^{-4\text{Im} \bar{k}_z c_\perp m} \\
& + \frac{1}{a} \frac{c_\perp}{a} \sin(3k_z c_\perp) (2c_\perp/a+1) e^{-3c_\perp/a} e^{-2\text{Im} \bar{k}_z c_\perp} \\
& \times (1+e^{-2\text{Im} \bar{k}_z c_\perp}) \sum_{m=0}^{\infty} e^{-4\text{Im} \bar{k}_z c_\perp m}, \quad (41)
\end{aligned}$$

$$\begin{aligned}
\tilde{\gamma}_2(k_z) & \equiv \text{Re} \sum_m \sum_{m'} \sum_{m''} e^{-2\text{Im} \bar{k}_z c_\perp (m+m'')} e^{i2k_z c_\perp (m-m''-\frac{1}{2})} \\
& \times \bar{\zeta}(m-m') \bar{\xi}(m'-m''-\frac{1}{2}) \\
& \approx \frac{2}{a} \frac{c_\perp}{a} [\sin(k_z c_\perp) + \sin(3k_z c_\perp)] e^{-2\text{Im} \bar{k}_z c_\perp} (c_\perp/a+1) \\
& \times e^{-3c_\perp/a} (1+e^{-2\text{Im} \bar{k}_z c_\perp}) \sum_{m=0}^{\infty} e^{-4\text{Im} \bar{k}_z c_\perp m}. \quad (42)
\end{aligned}$$

The above $\tilde{\alpha}(k_z)$, $\tilde{\beta}(k_z)$, $\tilde{\gamma}_1(k_z)$, and $\tilde{\gamma}_1(k_z)$ are also correct up to $e^{-3c_\perp/a}$. Now we have done the evaluation of $G_{21}^+ \Delta G_{11}^+ \Delta G_{22}^- + G_{22}^+ \Delta G_{11}^+ \Delta G_{21}^-$. Using Eqs.(39)-(42), we have

$$\begin{aligned}
& G_{21}^+ \Delta G_{11}^+ \Delta G_{22}^- + G_{22}^+ \Delta G_{11}^+ \Delta G_{21}^- \\
& = 2 \left[-\frac{1}{\pi} \text{Im} \bar{G}_1^+(k_y) \right] |\chi(k_x)|^2 |\chi(k_y)|^2 |\chi(k_z)|^2 e^{-2\text{Im} \bar{k}_z c_\perp} \\
& \times [\varepsilon_x^2 k_x \zeta(k_x) \tilde{\alpha}(k_z) + \varepsilon_y^2 k_y^2 \xi(k_x) \tilde{\alpha}(k_z) \\
& +\varepsilon_z^2 \xi(k_x) \tilde{\beta}(k_z) + \varepsilon_x \varepsilon_y k_y \zeta(k_x) \tilde{\alpha}(k_z) \\
& +\varepsilon_x \varepsilon_y k_x k_y \xi(k_x) \tilde{\alpha}(k_z) + \varepsilon_y \varepsilon_z k_y \xi(k_x) \tilde{\gamma}_1(k_z) \\
& +\varepsilon_y \varepsilon_z k_y \xi(k_x) \tilde{\gamma}_2(k_z) + \varepsilon_z \varepsilon_x k_x \xi(k_x) \tilde{\gamma}_2(k_z) \\
& +\varepsilon_z \varepsilon_x \zeta(k_x) \tilde{\gamma}_1(k_z)]. \quad (43)
\end{aligned}$$

The other four terms out of Eq.(28) can be obtained using the symmetry above without actual calculations. From Eq.(28), we note the other terms are

$$G_{22}^+ \Delta G_{12}^+ \Delta G_{22}^- = e^{-2\text{Im}\bar{k}_z c_\perp} \times [G_{21}^+ \Delta G_{11}^+ \Delta G_{21}^-; x \iff y], \quad (44)$$

where the notation $[G_{21}^+ \Delta G_{11}^+ \Delta G_{21}^-; x \iff y]$ means the same expression as $G_{21}^+ \Delta G_{11}^+ \Delta G_{21}^-$ with only $k_x \leftrightarrow k_y$, $\varepsilon_x \leftrightarrow \varepsilon_y$ exchanged. When keeping the same notation,

$$G_{21}^+ \Delta G_{12}^+ \Delta G_{21}^- = e^{2\text{Im}\bar{k}_z c_\perp} \times [G_{22}^+ \Delta G_{11}^+ \Delta G_{22}^-; x \iff y], \quad (45)$$

$$G_{21}^+ \Delta G_{12}^+ \Delta G_{22}^- + G_{22}^+ \Delta G_{12}^+ \Delta G_{21}^- = [G_{21}^+ \Delta G_{11}^+ \Delta G_{22}^- + G_{22}^+ \Delta G_{11}^+ \Delta G_{21}^-; x \iff y]. \quad (46)$$

The total photoemission intensity $I(\mathbf{k}, E, \omega)$ is the sum of permutative contributions (Eq.(28)) obtained above.

In the experiment of Zhou *et al.*'s [14], the spectral weight distribution has been represented by integrating $I(\mathbf{k}, E, \omega)$ for finite energy windows. From the weight distribution, they suggest the superposition of two perpendicular one-dimensional charged stripes for the underlying electronic structure. Other features such as the weight suppression along the d -wave nodal directions $\mathbf{k} = (\pm 1, \pm 1)$ including the Γ point does not seem easily explained, for which they propose a gap formation around $|k_x| \sim 1/4$ and $|k_y| \sim 1/4$. The origin of the gap, however, does not look very clear. Thus there may be left some rooms for another possibility. In our calculation, the integration of $I(\mathbf{k}, E, \omega)$ with respect to E can be readily done. From Eqs.(44), (45), and (46), the E -dependency is in $[-\frac{1}{\pi}\text{Im}\bar{G}_1^+(k_y)]$ or $[-\frac{1}{\pi}\text{Im}\bar{G}_1^+(k_x)]$ and through k_z . For $k_z = \sqrt{2(E + \omega) - k_x^2 - k_y^2}$, $|E| \lesssim 0.1$ eV from the band width, while $\omega \sim \mathcal{O}(10)$ eV in actual experiments. So we could approximate $k_z \approx \sqrt{2\omega - k_x^2 - k_y^2}$. Then the remaining integral is special,

$$\int dE \left[-\frac{1}{\pi} \text{Im}\bar{G}_1^+(k_{y(x)}) f(E) \right] = n_{k_{y(x)}}, \quad (47)$$

where $f(E)$ is the Fermi-distribution function. $[-\frac{1}{\pi}\text{Im}\bar{G}_1^+(k_{y(x)})]$ is the spectral function of the stripe, which determines its band structure. Because our starting point is the noninteracting chain (stripe), we should assume a suitable band dispersion relevant to the one-dimensional stripe. The corresponding band by the model calculation [24] from vertical stripes is very flat especially near $(\pi, 0)$, which is believed to have the one-dimensional character in the complicated real band dispersion. In the experiments [25], its band width is estimated about 30 meV and should be the integration energy window in our study. So we assume the band dispersion of the stripe to be $bk_y^2 - bk_f^2$ for \hat{y} -directed stripe, where $b \sim 0.18$ from $(\pi/l)^2 \sim 2.64$ eV ($l \sim 5.34\text{\AA}$). It should be noticed that, despite one-dimensional properties in the Nd-LSCO system, there have been no compelling evidences for Tomonaga-Luttinger-like electronic structure (i.e., such as the spin-charge separation)

in the stripe phase. Therefore, even if the matrix effects are explored based on one-dimensional stripes, we assume the Fermi-like momentum distribution $n_{k_{y(x)}}$, which is motivated by our interests in the polarization, photon energy and momentum dependencies of the ARPES intensity, not in the energy distribution curves (EDC's). Then we get the expression $\bar{I}(\mathbf{k}, \omega)$, defining $\bar{I}(\mathbf{k}, \omega) \equiv \int dE I(\mathbf{k}, E, \omega) f(E)$,

$$\begin{aligned} \bar{I}(\mathbf{k}, \omega) &\propto n_{k_y} |\chi(k_x)|^2 |\chi(k_z)|^2 e^{-\text{Im}\bar{k}_z c_\perp} \\ &\times [\varepsilon_x^2 \zeta(k_x)^2 \alpha(k_z) + \varepsilon_y^2 k_y^2 \xi(k_x)^2 \alpha(k_z) \\ &+ \varepsilon_z^2 \xi(k_x)^2 \beta(k_z) + 2\varepsilon_x \varepsilon_y k_y \xi(k_x) \zeta(k_x) \alpha(k_z) \\ &+ 2\varepsilon_y \varepsilon_z k_y \xi(k_x)^2 \gamma(k_z) + 2\varepsilon_z \varepsilon_x \xi(k_x) \zeta(k_x) \gamma(k_z)] \\ &+ e^{-2\text{Im}\bar{k}_z c} \times [k_x \iff k_y, \varepsilon_x \iff \varepsilon_y] \\ &+ 2n_{k_y} |\chi(k_x)|^2 |\chi(k_y)|^2 |\chi(k_z)|^2 e^{-2\text{Im}\bar{k}_z c_\perp} \\ &\times [\varepsilon_x^2 k_x \zeta(k_x) \tilde{\alpha}(k_z) + \varepsilon_y^2 k_y^2 \xi(k_x) \tilde{\alpha}(k_z) \\ &+ \varepsilon_z^2 \xi(k_x) \tilde{\beta}(k_z) + \varepsilon_x \varepsilon_y k_y \zeta(k_x) \tilde{\alpha}(k_z) \\ &+ \varepsilon_x \varepsilon_y k_x k_y \xi(k_x) \tilde{\alpha}(k_z) + \varepsilon_y \varepsilon_z k_y \xi(k_x) \tilde{\gamma}_1(k_z) \\ &+ \varepsilon_y \varepsilon_z k_y \xi(k_x) \tilde{\gamma}_2(k_z) + \varepsilon_z \varepsilon_x k_x \xi(k_x) \tilde{\gamma}_2(k_z) \\ &+ \varepsilon_z \varepsilon_x \zeta(k_x) \tilde{\gamma}_1(k_z)] \\ &+ [k_x \iff k_y, \varepsilon_x \iff \varepsilon_y] \\ &+ n_{k_y} |\chi(k_x)|^2 |\chi(k_y)|^2 |\chi(k_z)|^2 e^{-3\text{Im}\bar{k}_z c_\perp} \\ &\times [\varepsilon_x^2 k_x^2 \xi(k_y) \bar{\alpha}(k_z) + \varepsilon_y^2 \eta(k_y) \bar{\alpha}(k_z) \\ &+ \varepsilon_z^2 \xi(k_y) \bar{\beta}(k_z) + 2\varepsilon_x \varepsilon_y k_x \zeta(k_y) \bar{\alpha}(k_z) \\ &+ 2\varepsilon_y \varepsilon_z \zeta(k_y) \bar{\gamma}(k_z) + 2\varepsilon_z \varepsilon_x k_x \xi(k_y) \bar{\gamma}(k_z)] \\ &+ e^{2\text{Im}\bar{k}_z c_\perp} \times [k_x \iff k_y, \varepsilon_x \iff \varepsilon_y], \quad (48) \end{aligned}$$

where $[k_x \iff k_y, \varepsilon_x \iff \varepsilon_y]$ denotes the term right before it with $k_x \leftrightarrow k_y$ and $\varepsilon_x \leftrightarrow \varepsilon_y$ exchanged. According to Eq.(48), because of Γ (or $\text{Im}\bar{k}_z$), we expect to get an asymmetry in the weight distribution (with respect to k_x and k_y) depending on which is the first layer because the mean free path could govern only the first few layers in realistic situations. To compare with experiment [14], we average the spectra with respect to the stripe direction, i.e. for the two configurations in Fig.4.

From Eq.(48), we evaluate the spectral weight distribution for $\hat{\mathbf{E}} \perp xy$ and provide the results in Fig.5. Note the momentum distribution $n_{k_{y(x)}}$ readily gives two sets of Fermi surfaces defined by $|k_x| = 1/4$ and $|k_y| = 1/4$. In the figure, we have found two kinds of distributions depending on the photon energy. Figures 5(c) and 5(d) may be understood just as the superposition of two perpendicular sets, whereas Figs.5(a) and 5(b) are very interesting. As in the experiment, we can observe the spectral weight reduction along the d -wave nodal direction and also around the Γ point, and simultaneously the spectral confinement around $(0, \pm 1)$ and $(\pm 1, 0)$. This must be the geometric (interference) effect raised by the dipole matrix in our study. More clearly, when $\varepsilon_x = \varepsilon_y = 0$, $\bar{I}(\mathbf{k}, E)$ is determined by the functions $\beta(k_z)$, $\bar{\beta}(k_z)$, and

$\tilde{\beta}(k_z)$, of which $\bar{\beta}(k_z)$ must be dominant. Thus we can see that $\beta(k_z)$ is mainly attributed to $\bar{I}(\mathbf{k}, E)$, that is, $G_{22}^+ \Delta G_{11}^+ \Delta G_{22}^- + G_{21}^+ \Delta G_{12}^+ \Delta G_{21}^-$, which are the interference terms, not direct terms. If we try to explain the experiment based on the present results, a gap opening is not required and metallic stripes look enough to reproduce the observed weight distribution. Unfortunately, however, it is also found in our study that two types of spectral distributions appears alternatively depending on the photon energy. Experimentally, the intensity confinement near $(0, \pm 1)$ and $(\pm 1, 0)$ is robust when $\omega \sim 20$ eV, 30 eV, and 50 eV. In Fig.6, we give the spectral intensities at the Γ point for the photon energy ω .

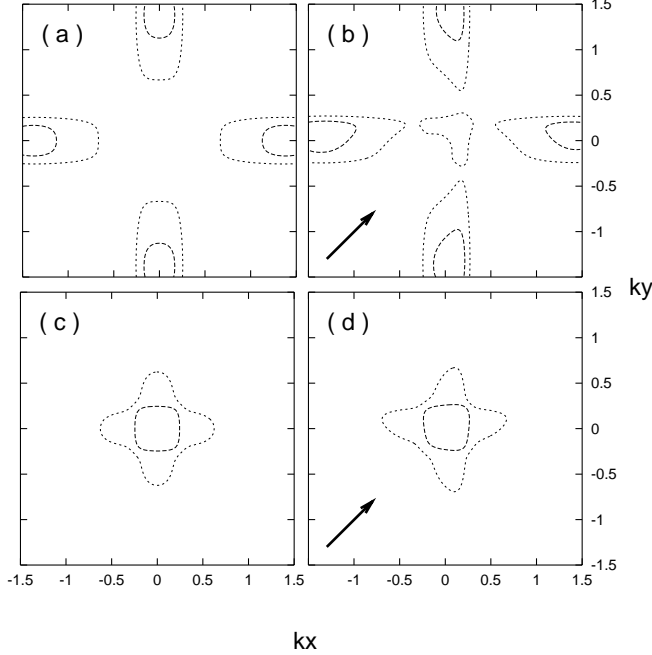


FIG. 5. Spectral weight distributions for the linearly polarized photon, especially perpendicular ((a) and (c)) or nearly perpendicular ((b) and (d)) to the layer are given. We have two kinds of distribution depending on the photon energy. (a) and (b) are for $\omega = 15(\pi/l)^2$ and (c) and (d) are for $\omega = 20(\pi/l)^2$. The arrow in the figures ((b) and (d)) denotes the direction of the in-plane electric field. $l/a = 2.5$ is used. The wave vector unit is π/l .

In Fig.7, the spectral distribution for $\hat{\mathbf{E}} \parallel xy$ is given, which is quite a different distribution from Fig.5. In the figure, the intensity at the Γ point is suppressed and there happen to be strong weights on the diagonals, i.e., $(0, 0)$ to $(\pm 1, \pm 1)$. According to the recent experiment [25], for $\hat{\mathbf{E}}$ parallel to the surface, weak intensities appear also in the diagonal directions in addition to the intensities at $(0, \pm 1)$ and $(\pm 1, 0)$, which would not be observed or observed weaker in the case of $\hat{\mathbf{E}}$ perpendicular to the surface. These additional complex structures have been suggested as the overlap of two-dimensional characters from stripe fluctuations on the simple one-dimensional

stripe picture, namely as part of the two dimensional Fermi surface. On the other hand, such fluctuations were not considered in our study.

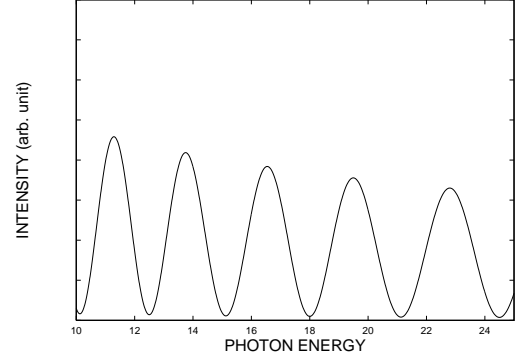


FIG. 6. Spectral intensities at the Γ point are given with respect to the photon energy when $\hat{\mathbf{E}} \perp xy$. The energy unit is $(\pi/l)^2$.

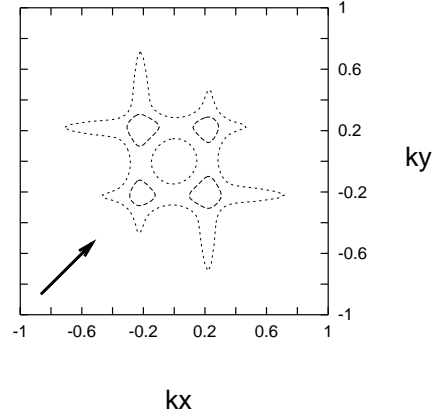


FIG. 7. The spectral weight distribution for $\hat{\mathbf{E}} \parallel xy$ for $\omega = 15(\pi/l)^2$. The arrow is the direction of $\hat{\mathbf{E}}$.

As shown in the figures, we do not stress the restricted agreement much. The stripe system, Nd-LSCO is a more complicated system compared to the chain system, PBCO. The real electronic structure may consist of both one-dimensional and two-dimensional components. This is very important and can explain why the present approach is good for PBCO, while less satisfactory for Nd-LSCO. The photon energy behavior in Figs.5 and 6, however, provides outlook for further studies along the present line. The first thing may be to go beyond the primary plane wave assumption for the photoelectron. The photoelectron wave function should be in principle calculated using the scattering theory including the surface. Also the excitation perpendicular to the stripes, neglected here, would introduce the surface Green's function [4]. We would then hopefully expect more correct transition matrix effects, and also more robust photon energy and polarization dependencies of the spectra. How-

ever, we do not mean here the matrix effect would be enough to understand experiments. We have regarded stripes as a collection of noninteracting metallic chains, but the interaction among the chains as well as the interaction between the chain and the two-dimensional background electronic structures may play a role essentially [24].

V. CONCLUSIONS

We have studied the dipole matrix effects of the photoemission in the system of linear metallic chains for two characteristic configurations. Assuming the chains (stripes) are perfectly one-dimensional by neglecting the transverse excitations and interchain interactions, we could write down the Green's function of the total system. Pendrey's formula enables us to manage the dipole matrix effects from knowledges of the single-particle Green's function. The calculations are very well controlled by small parameters $e^{-c_{\parallel}/a}$ or $e^{-c_{\perp}/a}$.

Interesting \mathbf{k} - and $\hat{\mathbf{E}}$ -dependencies in the photoemission spectra in PBCO system have been observed, which would be thought of as the transition matrix effects. We have evaluated the spectral intensities accounting for the dipole matrix in the system of chains based on the Luttinger model. PBCO is found to have one-dimensional chains which behave like Tomonaga-Luttinger liquid by recent ARPES studies. For the photoemission formula, we have adopted the Pendrey's formula. The relative intensities of separated holons and spinons depending on the wave vector \mathbf{k} (anisotropies), or the photon polarization (linear polarization, $\hat{\mathbf{E}}$) obtained in the study are found consistent with the recent experiments. It is also found that the present study would be applicable to another system having insulating Cu-O chains, SrCuO₂.

We have also considered the system more extended than PBCO. We have had interests in the static stripe phases observed in Nd-LSCO system. In experiments, their one-dimensional characters are observed from the spectral distribution in \mathbf{k} -space, but not perfectly understood from the stripe picture alone. We have studied its deviations arising from the dipole matrix effects. In the same way as for PBCO, we have calculated the integrated spectral distribution. We then found a distribution quite consistent with experiment (for $\hat{\mathbf{E}} \perp xy$), where the intensity around the Γ point or along the d -wave nodal directions is strongly suppressed. We have also found, however, another distribution showing a strong accumulation of intensities around the Γ point depending on the photon energy. In the result, two types of distributions appear alternatively as a function of photon energy. Such more or less shaky behaviors may be due to the simple plane wave assumption for the photoelectron state. For $\hat{\mathbf{E}} \parallel xy$, additional complex structures are more apparently observed in experiment. It is insisted that the system should consist of two components, both

one-dimensional and two-dimensional characters even in the static stripe phase in Nd-LSCO [25]. $\hat{\mathbf{E}}$ -dependent behaviors in our calculations, however, come from the interferences of noninteracting stripes (chains) and may be expected not fully justified in the stripe system. In the stripe system much two-dimensional characters induced by stripe fluctuations and interactions of the stripes with the two-dimensional background exist unlike a pure chain system. This is the reason that our study is successful for PBCO, whereas less successful in Nd-LSCO.

Finally, we may need to clarify the scope or limit for the present photoemission approach. We have thought of the noninteracting (noninteracting among chains and also between chains and the rest of the system) one-dimensional chains (stripes) for both PBCO and Nd-LSCO. Therefore, in such a sense, the matrix effects addressed in our study are purely geometric. This must be quite drastic approximations, but can be well consistent with our original purpose of studying the matrix effects. Further investigations for the dipole matrix effect are suggested to take into account better considerations for the stripes (allowing the transverse excitations) and thus leading to the surface Green's function, which would make it possible to describe the dynamical stripe phase too. We should also think of how good the plane wave for the photoelectron could be in these anisotropic systems.

ACKNOWLEDGEMENT

One of the authors (J.D.L.) acknowledges the fellowship from the Japan Society for the Promotion of Science. This work was supported by a Grant-in-aid for Scientific Research in the Priority Area "Novel Quantum Phenomena in Transition Metal Oxides" from the Ministry of Education, Science, Sports, and Culture and by the Special Coordination Fund for the Promotion of Science and Technology from the Science and Technology Agency.

-
- [1] Z.X. Shen and D.S. Dessau, Phys. Rep. **253**, 1 (1995); and references therein.
 - [2] C.O. Almbladh and L. Hedin in *Handbook on Synchrotron Radiation*, edited by E. Koch (North-Holland, Amsterdam, 1983) Vol. 1B, pp. 607-904.
 - [3] T. Matsushita *et al*, Phys. Rev. B **56**, 7687 (1997).
 - [4] A. Bansil and M. Lindroos, Phys. Rev. Lett. **83**, 5154 (1999).
 - [5] L. Hedin, J. Phys.: Condens. Matter **11**, R489, (1999).
 - [6] J.D. Lee, O. Gunnarsson, and L. Hedin, Phys. Rev. B **60**, 8034 (1999); J.D. Lee, Phys. Rev. B **61**, 8062 (2000).
 - [7] S. Tomonaga, Prog. Theor. Phys. **5**, 544 (1950); J.M. Luttinger, J. Math. Phys. **4**, 1154 (1963).

- [8] K. Takenaka *et al*, Phys. Rev. B **46**, 5833 (1992); M. Merz *et al*, Phys. Rev. B **55**, 9160 (1997); M. Takata *et al*, Physica C **263**, 340 (1996).
- [9] R. Fehrenbacher and T.M. Rice, Phys. Rev. Lett. **70**, 3471 (1993); A.I. Liechtenstein and I.I. Mazin, Phys. Rev. Lett. **74**, 1000 (1995).
- [10] T. Mizokawa *et al*, Phys. Rev. B **60**, 12335 (1999); For the double chain system of PrBa₂Cu₄O₈, the chain is actually metallic. See T. Mizokawa *et al*, Proceedings of the 12th International Symposium on Superconductivity (ISS-99), 173 (1999).
- [11] J. Zaanen and O. Gunnarsson, Phys. Rev. B **40**, 7391 (1989); V.J. Emery and S.A. Kivelson, Physica (Amsterdam) **209 C**, 597 (1993).
- [12] J.M. Tranquada *et al*, Nature **375**, 561 (1995); J.M. Tranquada, N. Ichikawa, and S. Uchida, Phys. Rev. B **59**, 14712 (1999).
- [13] C. Kim *et al*, Phys. Rev. B **56**, 15589 (1997).
- [14] X.J. Zhou *et al*, Science, **286**, 268 (1999).
- [15] J.B. Pendrey, Surface Science **57**, 679 (1976).
- [16] For the system such as the half-filled electron gas, the representation could be more satisfactory; See L. Hedin, J. Michiels, and J. Inglesfield, Phys. Rev. B **58**, 15565 (1998).
- [17] V. Meden and K. Schönhammer, Phys. Rev. B **46**, 15753 (1992); P. Kopietz, V. Meden, and K. Schönhammer, Phys. Rev. Lett. **74**, 2997 (1995).
- [18] B. Grevin *et al*, Phys. Rev. B **61**, 4334 (2000).
- [19] K. Takenaka *et al*, unpublished (2000).
- [20] In the Luttinger model, v_f^c/v_f is not a free parameter, but determined by α . That is, $v_f^c/v_f = \sqrt{1+2\eta}$ and $\eta = \frac{2\sqrt{\alpha(1+\alpha)/(1+2\alpha)}}{1-2\sqrt{\alpha(1+\alpha)/(1+2\alpha)}}$. For $\alpha \sim 0.6$, thus $v_f^c/v_f \sim 4.4$. This apparent discrepancy may be from the higher-dimensional character of the system. See J.D. Denlinger *et al*, Phys. Rev. Lett. **82**, 2540 (1999).
- [21] T. Noda, H. Eisaki, and S. Uchida, Science **286**, 265 (1999).
- [22] S.W. Cheong *et al*, Phys. Rev. Lett. **67**, 1791 (1991); T.E. Mason, G. Aeppli, and H.A. Mook, Phys. Rev. Lett. **68**, 1414 (1992).
- [23] A. Ino *et al*, J. Phys. Soc. Jpn, **68**, 1496 (1999); A. Ino *et al*, arXiv:cond-mat/0005370 (2000).
- [24] M.I. Salkola, V.J. Emery, and S.A. Kivelson, Phys. Rev. Lett. **77**, 155 (1996).
- [25] X.J. Zhou *et al*, arXiv:cond-mat/0009002 (2000).